THE JOURNAL OF PHYSICAL CHEMISTRY Letters

Letter

pubs.acs.org/JPCL

Raman Spectroscopy of Organic–Inorganic Halide Perovskites

Martin Ledinský,*[,†,‡] Philipp Löper,[†] Bjoern Niesen,[†] Jakub Holovský,[‡] Soo-Jin Moon,[§] Jun-Ho Yum,[§] Stefaan De Wolf,[†] Antonín Fejfar,[‡] and Christophe Ballif[†,§]

[†]Photovoltaics and Thin-Film Electronics Laboratory, Institute of Microengineering (IMT), Ecole Polytechnique Fédérale de Lausanne (EPFL), Neuchâtel 2000, Switzerland

[‡]Laboratory of Nanostructures and Nanomaterials, Institute of Physics, Academy of Sciences of the Czech Republic, Cukrovarnická 10, 162 00 Prague, Czech Republic

[§]CSEM PV-center, Neuchâtel 2000, Switzerland

ABSTRACT: Micro-Raman spectroscopy provides laterally resolved microstructural information for a broad range of materials. In this Letter, we apply this technique to triiodide ($CH_3NH_3PbI_3$), tribromide ($CH_3NH_3PbBr_3$), and mixed iodide–bromide ($CH_3NH_3PbI_{3-x}Br_x$) organic–inorganic halide perovskite thin films and discuss necessary conditions to obtain reliable data. We explain how to measure Raman spectra of pristine $CH_3NH_3PbI_3$ layers and discuss the distinct Raman bands that develop during moisture-induced degradation. We also prove unambiguously that the final degradation products contain pure PbI_2. Moreover, we describe $CH_3NH_3PbI_{3-x}Br_x$ Raman spectra and discuss how the perovskite crystallographic symmetries affect the Raman band intensities and spectral shapes. On the basis of the dependence of the Raman shift on the iodide-to-bromide ratio, we show that Raman spectroscopy is a fast and nondestructive method for the evaluation of the relative iodide-to-bromide ratio.

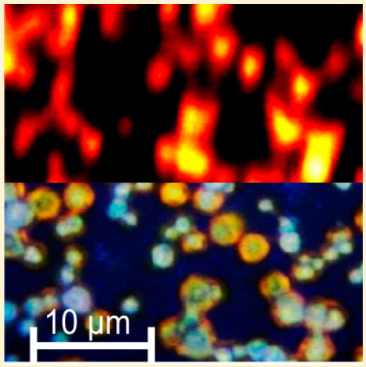

Thin-film solar cells based on organic–inorganic halide perovskite absorber layers are emerging as a high-performance photovoltaic technology. Since the first report on perovskite-based solar cells by Kojima et al.,[1] the conversion efficiency of these cells has increased rapidly to certified efficiencies up to 17.9%.[2,3] An important factor explaining this fast progress is found in the excellent semiconductor properties of $CH_3NH_3PbI_3$ perovskite films, displaying very high absorption coefficients in the visible part of the solar spectrum and a well-ordered microstructure of the deposited films, as evidenced by their sharp absorption edge.[4]

An advantage of organic–inorganic halide perovskites, compared to many other thin-film solar cell materials, is the fact that their band gap is readily tunable by either changing the atom at the halogen site or by changing the alkyl substituent at the ammonium cation.[5] Depending on the iodide-to-bromide ratio in the $CH_3NH_3PbI_{3-x}Br_x$ perovskite structure, the band gap energy varies from 1.57 to 2.23 eV.[6] This property is especially important for tandem solar cell applications, where a perovskite top cell of sufficiently wide band gap is stacked on a crystalline silicon (c-Si), copper indium gallium selenide or other bottom cell with a lower band gap energy.[7−11]

Unfortunately, perovskite solar cells typically degrade at moderate temperatures and upon moisture ingress. Insight into the fundamental principles underlying such degradation is of utmost importance to formulate mitigation strategies. For this, accurate characterization techniques are essential. Typically, the degradation process is nonhomogenous, often starting at the corner of a sample. One plausible degradation mechanism of $CH_3NH_3PbI_3$ thin films involves its decomposition in the presence of water vapor into CH_3NH_3, HI water solutions, and solid lead iodide PbI_2.[12] Regardless of the exact mechanism, the degradation is irreversible and finally results in a layer consisting of yellow PbI_2 platelets.[12] Optically, the degradation is evidenced as a bleached optical absorption in the orange–red part of the spectra,[4] visible to the naked eye, or more quantitatively by appropriate methods such as spectrophotometry, photothermal deflection spectroscopy (PDS), or Fourier-transform photocurrent spectroscopy (FTPS).[4] As the degradation induces a structural change, it can also be characterized with X-ray diffraction.[13] Unfortunately, all of these techniques have a low spatial resolution (typically in the mm to cm range) and do not permit locally resolved studies of the perovskite layer structural properties. However, precise mapping of microstructural information may be essential to unravel the fundamental degradation mechanisms as well as for probing of optoelectronic perovskite properties.

In this Letter, we present micro-Raman spectroscopy as a well-suited measurement technique to probe organic–inorganic halide perovskite layers locally on the micrometer scale. By using very low excitation laser intensities, we are able to obtain Raman spectra of pristine $CH_3NH_3PbI_3$ layers. After repeatedly measuring the same sample, we observe structural changes, which we correlate with local moisture-induced degradation of the perovskite film. On the basis of these results, we discuss the

Received: December 12, 2014
Accepted: January 13, 2015
Published: January 13, 2015

DOI: 10.1021/jz5026323
J. Phys. Chem. Lett. 2015, 6, 401−406

spectra of $CH_3NH_3PbI_{3-x}Br_x$ thin films and present a method to determine the Br-to-I ratio.

In Figure 1, we plot two typical Raman spectra of freshly prepared nondegraded $CH_3NH_3PbI_3$ perovskite films, measured at different positions on one of our samples. To avoid unintended sample degradation and/or undesired heating, the Raman measurements were taken using a laser excitation power of 10 μW, which is 2 orders of magnitude lower compared to "standard" semiconductor thin-film measurements such as on μc-Si:H thin films.[14] In the measured spectral region from 20 to 700 cm^{-1}, the Raman spectra reveal two distinct bands at 52 and 110 cm^{-1}. We observed these two bands systematically in all Raman spectra of pristine perovskite layers. When the samples were exposed to the ambient atmosphere for several hours, we observed the emergence of additional bands at 94 and 220 cm^{-1}. The relative intensity of these bands, compared to the band at 110 cm^{-1}, shows some position dependence. This indicates sample inhomogeneity on a μm scale, likely related to an increased degradation rate at grain boundaries.

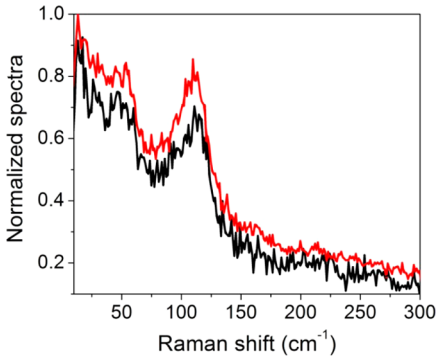

Figure 1. Raman spectra measured at two different positions on a pristine $CH_3NH_3PbI_3$ layer using a very low excitation laser power of 10 μW at 514.5 nm (spectra are normalized, without background correction).

When repeatedly measuring the Raman signal at the same position in ambient conditions, the spectra start to evolve, even for the very low laser excitation powers used here. Figure 2 depicts the spectral evolution induced by repeated measurements of a $CH_3NH_3PbI_3$ layer deposited on a c-Si wafer. The spectra were recorded consecutively without any additional delay time. The acquisition time of one spectrum was 60 s.

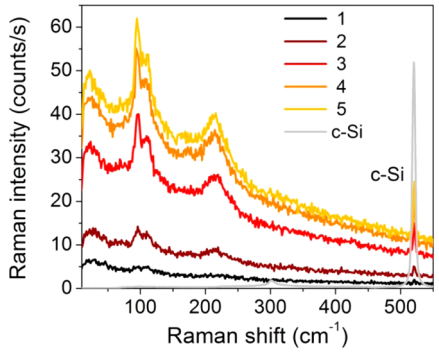

Figure 2. Five Raman spectra measured consecutively without any additional delay time at the same position of a $CH_3NH_3PbI_3$ layer at the excitation wavelength of 514.5 nm in ambient conditions (without any spectral correction or normalization).

With an increasing number of measurements, new peaks at 94, 220, and 520 cm^{-1} appear, whereas the band at 52 cm^{-1} vanishes. In addition, the absolute magnitude of these Raman bands and also the background signal increase. This phenomenon is very pronounced at 520 cm^{-1}, which is the well-known signature of the c-Si substrate band. The increasing intensity of this c-Si peak clearly indicates that the perovskite layer becomes increasingly transparent for the light of the excitation laser with a wavelength of 514.5 nm, such that more photons reach the c-Si substrate, creating c-Si Raman photons.

This increased transparency corresponds well to degradation by air moisture, as discussed in ref 4. There, it was shown that due to degradation, the band gap of the $CH_3NH_3PbI_3$ material increases from ~1.5 to 2.4 eV. In Figure 3, we show PDS absorptance spectra at several degradation states.

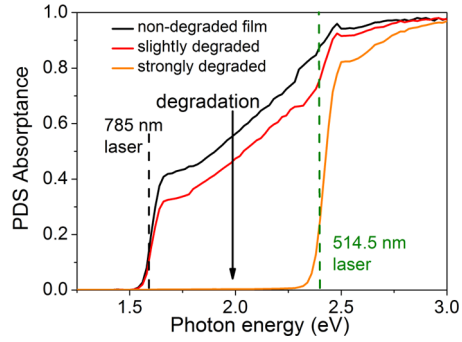

Figure 3. PDS absorptance spectra of $CH_3NH_3PbI_3$ layers at various degradation states. As the layers degrade, their absorptance is significantly reduced for wavelengths higher than 500 nm. The green and black lines indicate the excitation laser wavelengths used for these experiments (514.5 and 785 nm, respectively).

The green line in Figure 3 indicates the wavelength of the 514.5 nm laser. Due to the degradation of the perovskite layer, the $CH_3NH_3PbI_3$ layer absorption at this wavelength decreases significantly, resulting in increased transparency. Hence, a higher Raman signal from the c-Si substrate is detected during the measurements.

It is noteworthy that the Raman signal in the region of 50–250 cm^{-1} is present for all measurements and there is no visual change of the sample during the experiment. Hence, we are not substantially removing material from the perovskite layer during the measurements. As the film becomes more transparent, the penetration depth of the laser and thus the Raman interaction volume increase, leading to an intensity increase of all Raman bands.[14] Simultaneously, the structure of the film locally changes, as evidenced by the appearance of new Raman bands.

In order to prove that the observed degradation is caused by moisture ingress, we compare the Raman spectra of the degraded perovskite layer with that of pure PbI_2, which is deemed to be one of the degradation-reaction products.[12] This comparison is given in Figure 4, where it can be seen that during degradation, the pristine $CH_3NH_3PbI_3$ perovskite Raman spectrum changes to resemble closely that of a pure PbI_2 thin film. The basic modes and measured frequencies are indicated in the graph. All observed Raman bands match well those described for bulk PbI_2 crystals in the literature (black dashed lines).[15,16] Very good agreement is also seen with the Raman spectra of a PbI_2 layer (prepared by the same method) reported in ref 17. On the basis of these results, we confirm that one of the final products of the Raman laser-induced

DOI: 10.1021/jz5026323
J. Phys. Chem. Lett. 2015, 6, 401–406

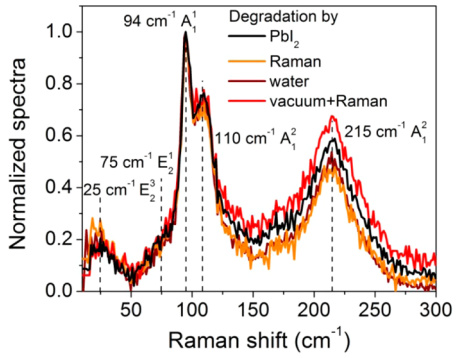

Figure 4. Raman spectra of degraded $CH_3NH_3PbI_3$ layers. The layers were intentionally degraded either by exposure to moisture, by the Raman excitation laser in ambient air, or by the Raman excitation laser in vacuum (residual pressure of several Pa). For comparison, the spectrum of an as-prepared PbI_2 thin film is also plotted. All spectra are normalized, following linear background subtraction, measured with a 514.5 nm Raman laser.

degradation process is PbI_2. The sample degradation under ambient conditions without illumination is by orders of magnitude slower, and its role during these experiments may be neglected.

To gain more insight into the degradation mechanisms, we also performed Raman measurements in vacuum. Again, the Raman spectra of the degraded films match closely those for PbI_2 (Figure 4). From this, we conclude that the layers degrade even without the presence of additional water vapor. It appears that under strong illumination by the laser beam and higher temperatures, the degradation is significantly accelerated. It is important to point out that the temperature itself cannot be the sole cause of the perovskite degradation to PbI_2, as was proven by thermogravimetric analysis.[13]

Intriguingly, the Raman spectra of our *degraded* perovskite layers feature all spectral signatures reported recently for presumably *pristine* $CH_3NH_3PbI_3$ perovskite films,[18,19] which are mainly the sharp and broad bands at 94 and 250 cm^{-1}, respectively. This similarity and 30 times higher Raman laser intensity used in their study suggest that these earlier results were most probably obtained from at least partially degraded perovskite layers. The Raman spectra reported in refs 18 and 19 were measured with a 532 nm laser excitation; therefore, the spectral shape of PbI_2 Raman spectra may be changed due to different resonant Raman conditions. However, we do not observe these Raman bands in pristine films (see Figure 1 with no Raman bands at 94 and 250 cm^{-1}). On the basis of the data given in Figure 4, we rather attribute the bands at 94 and 250 cm^{-1} to PbI_2. The broad band at ~250 cm^{-1} has been observed for PbI_2 crystals and has been interpreted as a resonantly enhanced second-order signal of the 120 cm^{-1} band.[15] Moreover, $CH_3NH_3PbI_3$ Raman spectra presented in Figure 1 are in very good agreement with density functional theory calculations reported in ref 18, in which a band is predicted at 50 cm^{-1} and there is no signal around 250 cm^{-1}.

After establishing a measurement protocol for pristine and degraded $CH_3NH_3PbI_3$ layers, we performed Raman measurements on $CH_3NH_3PbI_{3-x}Br_x$ mixed halide perovskites. For $CH_3NH_3PbI_{3-x}Br_x$ layers, strong photoluminescence signal excited by a 514.5 nm laser makes Raman measurements at this excitation wavelength impossible. For this reason, we used a 785 nm laser for $CH_3NH_3PbI_{3-x}Br_x$ perovskites layer characterization. As the photon energy at this excitation wavelength is not sufficiently high to be absorbed in the mixed perovskite layer, no photoluminescence signal is found, the layer is not heated by the laser, and no structural changes are detected during the measurement. This is different for pure $CH_3NH_3PbI_3$ films as they absorb at 785 nm (see the black dashed line in Figure 3) and a strong photoluminescence occurs.[20] To avoid laser-induced degradation during the measurement, the optimal excitation wavelength for $CH_3NH_3PbI_3$ layers seems to be 830 nm. However, this wavelength is rarely available in commercially available micro-Raman spectrometers.

Figure 5 shows the measured Raman spectra of mixed halide perovskites, for five Br-to-I ratios. The pure $CH_3NH_3PbI_3$ and

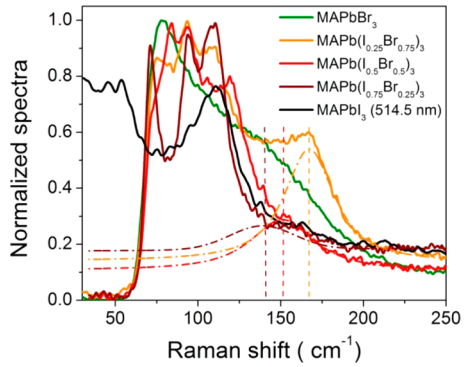

Figure 5. Raman spectra of $CH_3NH_3PbI_{3-x}Br_x$ mixed halide perovskite layers measured using a 785 nm excitation laser. A holographic filter with a cutoff edge at 70 cm^{-1} was used. The $CH_3NH_3PbI_3$ spectrum was measured using a 514.5 nm excitation layer and a 20 cm^{-1} Bragg filter. All spectra are normalized, without background correction. The horizontal dashed lines indicate the peak position of the most energetic Raman band for each Br-to-I ratio, obtained by fitting the spectra with Gaussian curves.

$CH_3NH_3PbBr_3$ perovskite thin films exhibit Raman spectra with broad peaks of low intensity compared to the mixed perovskites. Such peaks are typical for crystals with cubic symmetry, which have no Raman-active phonon modes. Indeed, $CH_3NH_3PbBr_3$ has cubic symmetry at room temperature,[5] and the Raman spectra published in ref 5 are in good agreement with our measurements of $CH_3NH_3PbBr_3$ thin films. Because the Raman spectrum of lead bromide ($PbBr_2$, ref 21) consists of several Raman bands and is clearly different from the $CH_3NH_3PbBr_3$ Raman spectrum, we conclude that there is no residual lead bromide in the perovskite film.

Mixed $CH_3NH_3PbI_{3-x}Br_x$ materials do not possess a cubic symmetry as the halide ions (I, Br) occupy the octahedron corners randomly. Consequently, phonon vibrations are active in the Raman spectra. All spectra exhibit several sharp Raman bands that are significantly stronger than those for pure halide perovskites. Mixed halide perovskite Raman bands undergo a red shift with increasing Br concentration. To quantitatively describe this effect, we fitted the most energetic phonon band of the mixed halide layers with a Gaussian curve (Figure 5). Due to the same structural symmetry of all mixed halide perovskites, it is reasonable to assume that this band represents the same vibrational mode. With increasing Br content, the Raman band positions are (139 ± 6), (151 ± 2), and (167 ± 1) cm^{-1}, for the three shown mixed-halide perovskite films. This shift of the Raman bands is caused by the lower molecular weight of the Br atom as compared to the I atom. The phonon

DOI: 10.1021/jz5026323
J. Phys. Chem. Lett. 2015, 6, 401−406

energy or Raman shift is, in the case of mixed halide perovskites, inversely proportional to the square root of the halide atom mass (assuming negligible difference in the Pb−I and Pb−Br bond strengths). Therefore, with increasing Br content, the Raman bands red shift. This effect can be used to estimate the Br-to-I ratio in mixed halide perovskite films. The iodide concentration C_I may be calculated from the formula (the first-order expansion of the inverse square root dependence of the Raman shift on the halide masses)

$$P_{I+Br} = P_{Br}(1 - \alpha C_I)$$

where P_{I+Br} and P_{Br} are the Raman band positions of mixed I + Br perovskite layers and pure bromide perovskite layers, respectively, and α is the Raman shift coefficient. To calculate α, we used the positions of the fitted mixed halide perovskite Raman bands as well as the position of the corresponding band of pure bromide perovskite layers at (180 ± 5) cm^{-1}, obtained at high pressure (when the cubic symmetry was canceled and phonon bands became visible).[5] On the basis of these results, the Raman shift coefficient was determined as

$$\alpha = 0.31 \pm 0.03.$$

The symmetry group of the $CH_3NH_3PbI_3$ crystal is still widely discussed in the literature. A tetragonal symmetry (with the inorganic octahedral tilt of roughly 16°)[22,23] was identified at room temperature by X-ray diffraction,[13] while transmission electron microscopy measurements suggested a pseudocubic structure.[13] The phonon modes of $CH_3NH_3PbI_3$ crystals are only weakly active, such that no sharp signatures were detected in the Raman spectra. The results of our Raman measurements therefore suggest that $CH_3NH_3PbI_3$ has a cubic symmetry. This is most probably caused by heating of the perovskite film by the laser light absorption; once the temperature exceeds 57 °C, the structure of the $CH_3NH_3PbI_3$ changes from the tetragonal to the cubic phase.[13] From symmetry considerations, the spectral shape of both the pure Br and I perovskites should be very similar. Therefore, the broad bands detected at 110 cm^{-1} for $CH_3NH_3PbI_3$ and at 150 cm^{-1} for $CH_3NH_3PbBr_3$ should have the same vibrational origin. This allows us to directly estimate the Raman shift coefficient as

$$\alpha = 0.27 \pm 0.05.$$

We note that the Raman band position may change on the order of several cm^{-1} for different excitation wavelengths, such that this number has to be treated with caution. Nevertheless, this result is in excellent agreement with the Raman shift coefficient calculated with higher precision from the mixed halide Raman spectra. On the basis of these considerations, we can predict the positions of all Raman bands observed for mixed halides perovskites films for any Br-to-I ratio. For example, the band at 52 cm^{-1} measured for $CH_3NH_3PbI_3$ should have a corresponding band for $CH_3NH_3PbBr_3$ at 75 cm^{-1} (calculated with a Raman shift coefficient $\alpha = 0.31$). This band can indeed be observed in the measured $CH_3NH_3PbBr_3$ spectra (see Figure 5), partially hidden by the absorption edge of the Raman holographic filter but still detectable.

Thanks to the high lateral resolution of Raman microspectroscopy, the chemical information may be obtained from submicrometer large structures, as demonstrated in Figure 6. The measured $CH_3NH_3PbBr_3$ layer is not complete (as in ref 24); it consists of crystal grains with a size of 1−3 μm (see Figure 6b). The intensity of the $CH_3NH_3PbBr_3$ Raman band at 149 cm^{-1} is plotted in Figure 6a. All individual grains are clearly

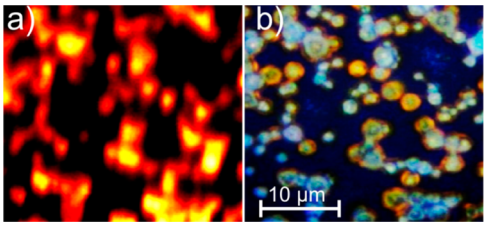

Figure 6. (a) Intensity of the $CH_3NH_3PbBr_3$ Raman band at 149 cm^{-1}. The black color indicates no Raman signal; maximal Raman intensities are marked by yellow. An excitation wavelength of 785 nm was used, and the sample was scanned in steps of 200 nm in both the *x* and *y* directions. (b) The same spot on the sample imaged by optical microscope shows individual $CH_3NH_3PbBr_3$ crystals of diameters down to 1 μm.

resolved in the Raman map, which leads to a rough estimation of the lateral resolution of 1 μm. Precise mapping of microstructural information may be essential to unravel the fundamental degradation mechanisms as well as for probing of perovskite optoelectronic properties. These results indicate that the high spatial resolution of Raman microspectroscopy enables the detection of local inhomogeneities of the Br-to-I concentration ratio. Such spatially resolved information may elucidate, for example, the reversible photoinduced trap formation in mixed halide perovskites.[25]

In summary, Raman spectra of pristine $CH_3NH_3PbI_3$ thin films were presented. The structural changes under 514.5 nm laser illumination were studied in detail, and degradation was identified to cause the conversion from $CH_3NH_3PbI_3$ to PbI_2. Because the same degradation process was found in vacuum, the water-based model did not play the main role here. In order to avoid Raman laser-induced degradation, an 830 nm excitation laser is recommended. Thanks to the high lateral resolution and sensitivity of Raman spectroscopy to the degradation product PbI_2, this technique is promising for local degradation studies. Finally, it was shown that for $CH_3NH_3PbI_{3-x}Br_x$ mixed halide perovskite layers, we can predict from the shift of the Raman bands the ratio of the iodine-to-bromine atoms in the perovskite layer. Therefore, Raman mapping is a powerful tool for studying local inhomogeneities of the halide concentrations on a submicrometer scale.

■ EXPERIMENTAL METHODS

$CH_3NH_3PbI_3$ films were prepared on glass substrates or double-side polished c-Si wafers. Glass substrates were cleaned ultrasonically in isopropyl alcohol, whereas c-Si wafers were dipped in a solution of 5% HF in H_2O for 60 s immediately before perovskite layer preparation, in order to remove native silicon oxide. PbI_2 was purchased from Sigma-Aldrich, and the material CH_3NH_3I was synthesized following the procedure described in ref 26. $CH_3NH_3PbI_3$ perovskite layers were deposited using a sequential deposition method described in ref 27. PbI_2 was dissolved in *N*,*N*-dimethylformamide at a concentration of 461 mg mL^{-1} at 70 °C. This PbI_2 solution was then spin-coated on glass at 6500 rpm for 30 s. After drying the PbI_2 coated glass at 70 °C for 10 min, the substrate was dipped in a solution of CH_3NH_3I in isopropyl alcohol (10 mg mL^{-1}) for 30 s, rinsed with isopropyl alcohol, and annealed at 70 °C for 10 min.

We prepared $CH_3NH_3PbI_{3-x}Br_x$ layers by a one-step deposition process. $PbBr_2$ and CH_3NH_3Br were purchased

DOI: 10.1021/jz5026323
J. Phys. Chem. Lett. 2015, 6, 401−406

from Sigma-Aldrich. The precursor solutions were composed of equivalent molar amounts of organic and inorganic components (CH_3NH_3I to PbI_2 and CH_3NH_3Br to $PbBr_2$, respectively). By mixing the precursor solutions, the final Br-to-I ratio was controlled, as reported in refs 6 and 28. The $CH_3NH_3PbI_{3-x}Br_x$ solutions were spin-coated on glass substrates and annealed on a hot plate at 80 °C for 10 min. All samples were prepared in a N_2 atmosphere.

Raman spectra were measured in backscattering geometry using a microspectroscopic Raman setup equipped with a 514.5 nm excitation laser (RM1000, Renishaw) and an In-Via REFLEX setup (Renishaw) with a 785 nm excitation laser. Samples were measured at room temperature and in ambient air. Raman spectra were measured for 60 s by a 50× objective, resulting in a laser spot diameter of 1 μm on the sample. For measurements with the 514.5 nm laser, Bragg filters were used to block the excitation laser line, allowing Raman measurements from 20 cm^{-1}, and a homemade vacuum chamber enabled us to measure Raman spectra at pressures down to several Pa.

Absorptance spectra of samples on glass at different degradation states due to moisture ingress were measured by PDS. A monochromator-based spectrometer with a 150 W xenon lamp was used for these measurements, while the samples were immersed in temperature-sensitive Fluorinert FC-72 (refractive index of 1.25), preventing moisture ingress and degradation of the sample during the measurement. Prior to Raman and PDS measurements, the perovskite layers were stored in a N_2 atmosphere in the dark.

AUTHOR INFORMATION

Corresponding Author

*E-mail: ledinsky@fzu.cz.

Notes

The authors declare no competing financial interest.

ACKNOWLEDGMENTS

The project comprising this work was evaluated by the Swiss National Science Foundation and funded by Nano-Tera.ch with Swiss Confederation financing and by the Swiss Federal Office of Energy, under Grant SI/501072-01. This work was also supported by the Czech Science Foundation Project 14-15357S and by the Czech Ministry of Education, Youth and Sports Project LM2011026. M.L. acknowledges the SCIEX Project 12.372 for financial support.

REFERENCES

(1) Kojima, A.; Teshima, K.; Shirai, Y.; Miyasaka, T. Organometal Halide Perovskites as Visible-Light Sensitizers for Photovoltaic Cells. *J. Am. Chem. Soc.* **2009**, *131*, 6050−6051.

(2) Zhou, H.; Chen, Q.; Li, G.; Luo, S.; Song, T.; Duan, H.-S.; Hong, Z.; You, J.; Liu, Y.; Yang, Y. Interface Engineering of Highly Efficient Perovskite Solar Cells. *Science* **2014**, *345*, 542−546.

(3) Jeon, N. J.; Noh, J. H.; Yang, W. S.; Kim, Y. C.; Ryu, S.; Seo, J.; Seok, S. I. Compositional Engineering of Perovskite Materials for High-Performance Solar Cells. *Nature* **2015**, DOI: 10.1038/nature14133.

(4) De Wolf, S.; Holovsky, J.; Moon, S.-J.; Loeper, P.; Niesen, B.; Ledinsky, M.; Haug, F.-J.; Yum, J.-H.; Ballif, C. Organometallic Halide Perovskites: Sharp Optical Absorption Edge and Its Relation to Photovoltaic Performance. *J. Phys. Chem. Lett.* **2014**, *5*, 1035−1039.

(5) Matsuishi, K.; Ishihara, T.; Onari, S.; Chang, Y. H.; Park, C. H. Optical Properties and Structural Phase Transitions of Lead-Halide Based Inorganic−Organic 3D and 2D Perovskite Semiconductors under High Pressure. *Phys. Status Solidi B* **2004**, *241*, 3328−3333.

(6) Noh, J. H.; Im, S. H.; Heo, J. H.; Mandal, T. N.; Seok, S. I. Chemical Management for Colorful, Efficient, and Stable Inorganic−Organic Hybrid Nanostructured Solar Cells. *Nano Lett.* **2013**, *13*, 1764−1769.

(7) Snaith, H. J. Perovskites: The Emergence of a New Era for Low-Cost, High-Efficiency Solar Cells. *J. Phys. Chem. Lett.* **2013**, *4*, 3623−3630.

(8) Loeper, P.; Moon, S.-J.; Martin de Nicolas, S.; Niesen, B.; Ledinsky, M.; Nicolay, S.; Bailat, J.; Yum, J.-H.; De Wolf, S.; Ballif, C. Organic−Inorganic Halide Perovskite/Crystalline Silicon Four-Terminal Tandem Solar Cells. *Phys. Chem. Chem. Phys.* **2015**, *17*, 1619−1629.

(9) Loeper, P.; Niesen, B.; Moon, S.; Martin de Nicolas, S.; Holovsky, J.; Remes, Z.; Ledinsky, M.; Haug, F.; Yum, J.; De Wolf, S.; et al. Organic−Inorganic Halide Perovskites: Perspectives for Silicon-Based Tandem Solar Cells. *IEEE J. Photovoltaics* **2014**, *6*, 1545−1551.

(10) Todorov, T.; Gershon, T.; Gunawan, O.; Sturdevant, C.; Guha, S. Perovskite−Kesterite Monolithic Tandem Solar Cells with High Open-Circuit Voltage. *Appl. Phys. Lett.* **2014**, *105*, 173902.

(11) White, T. P.; Lal, N. N.; Catchpole, K. R. Tandem Solar Cells Based on High-Efficiency c-Si Bottom Cells: Top Cell Requirements for >30% Efficiency. *IEEE J. Photovoltaics* **2014**, *4*, 208−214.

(12) Frost, J. M.; Butler, K. T.; Brivio, F.; Hendon, C. H.; van Schilfgaarde, M.; Walsh, A. Atomistic Origins of High-Performance in Hybrid Halide Perovskite Solar Cells. *Nano Lett.* **2014**, *14*, 2584−2590.

(13) Baikie, T.; Fang, Y.; Kadro, J. M.; Schreyer, M.; Wei, F.; Mhaisalkar, S. G.; Graetzel, M.; White, T. J. Synthesis and Crystal Chemistry of the Hybrid Perovskite (CH_3NH_3) PbI_3 for Solid-State Sensitised Solar Cell Applications. *J. Mater. Chem. A* **2013**, *1*, 5628−5641.

(14) Ledinský, M.; Moulin, E.; Bugnon, G.; Ganzerová, K.; Vetushka, A.; Meillaud, F.; Fejfar, A.; Ballif, C. Light Trapping in Thin-Film Solar Cells Measured by Raman Spectroscopy. *Appl. Phys. Lett.* **2014**, *105*, 111106.

(15) Nakashima, S. Raman Study of Polytypism in Vapor-Grown PbI_2. *Solid State Commun.* **1975**, *16*, 1059−1062.

(16) Capozzi, V.; Fontana, A.; Fontana, M.; Mariotto, G.; Montagna, M.; Viliani, G. Raman-Scattering in PbI_2. *Nuovo Cimento Soc. Ital. Fis., B* **1977**, *39*, 556−568.

(17) Condeles, J. F.; Ando, R. A.; Mulato, M. Optical and Structural Properties of PbI_2 Thin Films. *J. Mater. Sci.* **2008**, *43*, 525−529.

(18) Quarti, C.; Grancini, G.; Mosconi, E.; Bruno, P.; Ball, J. M.; Lee, M. M.; Snaith, H. J.; Petrozza, A.; De Angelis, F. The Raman Spectrum of the $CH_3NH_3PbI_3$ Hybrid Perovskite: Interplay of Theory and Experiment. *J. Phys. Chem. Lett.* **2014**, *5*, 279−284.

(19) Grancini, G.; Marras, S.; Prato, M.; Giannini, C.; Quarti, C.; De Angelis, F.; De Bastiani, M.; Eperon, G. E.; Snaith, H. J.; Manna, L.; et al. The Impact of the Crystallization Processes on the Structural and Optical Properties of Hybrid Perovskite Films for Photovoltaics. *J. Phys. Chem. Lett.* **2014**, *5*, 3836−3842.

(20) Deschler, F.; Price, M.; Pathak, S.; Klintberg, L. E.; Jarausch, D.-D.; Higler, R.; Huettner, S.; Leijtens, T.; Stranks, S. D.; Snaith, H. J.; et al. High Photoluminescence Efficiency and Optically Pumped Lasing in Solution-Processed Mixed Halide Perovskite Semiconductors. *J. Phys. Chem. Lett.* **2014**, *5*, 1421−1426.

(21) Plekhanov, V. G. Lead Halides: Electronic Properties and Applications. *Prog. Mater. Sci.* **2004**, *49*, 787−886.

(22) Bretschneider, S. A.; Weickert, J.; Dorman, J. A.; Schmidt-Mende, L. Research Update: Physical and Electrical Characteristics of Lead Halide Perovskites for Solar Cell Applications. *APL Mater.* **2014**, *2*, 040701.

(23) Stoumpos, C. C.; Malliakas, C. D.; Kanatzidis, M. G. Semiconducting Tin and Lead Iodide Perovskites with Organic Cations: Phase Transitions, High Mobilities, and Near-Infrared Photoluminescent Properties. *Inorg. Chem.* **2013**, *52*, 9019−9038.

DOI: 10.1021/jz5026323
J. Phys. Chem. Lett. 2015, 6, 401−406

(24) Tan, Z.-K.; Moghaddam, R. S.; Lai, M. L.; Docampo, P.; Higler, R.; Deschler, F.; Price, M.; Sadhanala, A.; Pazos, L. M.; Credgington, D.; et al. Bright Light-Emitting Diodes Based on Organometal Halide Perovskite. *Nat. Nanotechnol.* **2014**, *9*, 687−692.
(25) Hoke, E. T.; Slotcavage, D. J.; Dohner, E. R.; Bowring, A. R.; Karunadasa, H. I.; McGehee, M. D. Reversible Photo-Induced Trap Formation in Mixed-Halide Hybrid Perovskites for Photovoltaics. *Chem. Sci.* **2014**, *6*, 613−617.
(26) Im, J.-H.; Chung, J.; Kim, S.-J.; Park, N.-G. Synthesis, Structure, and Photovoltaic Property of a Nanocrystalline 2H Perovskite-Type Novel Sensitizer $(CH_3CH_2NH_3)PbI_3$. *Nanoscale Res. Lett.* **2012**, *7*, 353.
(27) Burschka, J.; Pellet, N.; Moon, S.-J.; Humphry-Baker, R.; Gao, P.; Nazeeruddin, M. K.; Graetzel, M. Sequential Deposition as a Route to High-Performance Perovskite-Sensitized Solar Cells. *Nature* **2013**, *499*, 316−319.
(28) Sadhanala, A.; Deschler, F.; Thomas, T. H.; Dutton, S. E.; Goedel, K. C.; Hanusch, F. C.; Lai, M. L.; Steiner, U.; Bein, T.; Docampo, P.; et al. Preparation of Single-Phase Films of $CH_3NH_3Pb(I_{1-x}Br_x)_3$ with Sharp Optical Band Edges. *J. Phys. Chem. Lett.* **2014**, *5*, 2501−2505.

DOI: 10.1021/jz5026323
J. Phys. Chem. Lett. 2015, 6, 401−406